How to cite: *Angew. Chem. Int. Ed.* **2025**, *64*, e202422923
doi.org/10.1002/anie.202422923

Physical Chemistry **Very Important Paper**

Polarization-Induced Quantum Confinement of Negative Charge Carriers by Organic Nanoporous Frameworks

*Ritaj Tyagi and Vamsee K. Voora**

Abstract: We characterize the attachment of excess-electrons to organic nanoporous systems such as molecular nanohoops and models of covalent organic frameworks (COFs) using many-body methods. *All* the nanopore systems exhibit diffuse electronic states where the excess-electron is bound to the molecular scaffold via long-range polarization forces, and the excess-electron is predominantly localized in the interior of the nanopore or away from the molecular scaffold. Such "nanopore-bound" states show an enhanced electron-transfer coupling compared to more strongly-bound skeletal-states (or valence-bound states), where the excess-electron is confined to the molecular skeleton. For 1D assemblies of nanohoops, the bands formed from nanopore-bound states have a consistent nearly-free-electron character, indicating an efficient excited-state pathway for charge-carriers, while the bands from skeletal-states have higher effective mass along certain lattice directions. The nanopore-bound states show distinct size-dependent variations in electron affinities compared to skeletal-states and previously observed molecular quantum corral states. We conclude that nanopore-bound states emerge from polarization-induced quantum confinement, forming a distinct common feature of organic nanoporous matter with potential for efficient electron-transport.

Introduction

Emergence of molecular electronic states that provide alternative pathways for electron transport can immensely impact the design of organic electronics. Traditionally, organic-matter based electronic transport is realized via molecular orbitals where the excess-electron (or hole) is confined within valence orbitals of the molecular scaffold. In such valence or skeletal-bound states, the electron-transfer integrals often decay rapidly with intermolecular separation. It could therefore be promising to consider electronic pathways where the electronic density of the excess charge is localized away from the molecular scaffold. Inspiration for such states includes the emergence of electronic states by molecular nanoarchitectures deposited on metal surfaces.[1,2] These emergent states arise from molecular quantum confinement or corraling of surface electrons of metals, and are observed via scanning tunneling microscopy (STM).[3] Nonskeletal densities can also be found in the case of layered materials such as electrides, for example, $[Ca_2N]^+[e^-]$, where the electrons take up the role of counter anions, and are localized within the interlayer spaces.[4] Other inspirations for nonskeletal states include nonvalence electronic states where negative charge carriers, that is, excess electrons, are bound to the molecule via a combination of long-range correlation and electrostatic effects.[5] Such nonvalence states have been observed in organic molecules with (fused) aromatic rings such as C_6F_6, polycyclic aromatic hydrocarbons (PAHs) and fullerenes.[5–8] Some of these nonvalence states have been observed in gas-phase[9,10] or upon deposition on metal surfaces.[11–14]

In this work, we explore the existence of similar nonvalence excess-electron states in porous organic frameworks where individual aromatic organic rings are attached covalently, unlike the fused rings of PAHs or fullerenes, to form either closed macrocyclic rings, which are referred to as nanohoops,[15] or form extended networks, which are commonly known as covalent organic frameworks (COFs).[16,17] These nanohoops and COFs contain nanopores with radii starting from 0.6 nm and extending up to several nanometers, and they have gained immense interest in areas of organic electronics, drug delivery, and nanoscale sensing.[18–24] The nanohoops can be functionalized, leading to tunability of fundamental gaps, enhancement of electron affinity, or induction of spin polarization, thereby expanding the range of applications in electronics, photonics, and spintronics.[18–20,25–27]

As examples of nanohoops, in this work, we consider the cycloparaphenylenes (CPPs), their polyfluorinated analogues (PFCPPs), and the honeycombenes [HC], see Figure 1. The CPPs are widely studied nanohoops and extensively explored together with fullerenes as host-guest complexes for optoelectronic applications[19,20,30–33] The CPPs are already known to exhibit distinct electronic properties compared to their linear counterparts. For example, the HOMO-LUMO gap of CPPs

[*] R. Tyagi, V. K. Voora
Department of Chemical Sciences, Tata Institute of Fundamental Research, Homi Bhabha Road, Colaba, Mumbai 400005, India
E-mail: vamsee.voora@tifr.res.in

Additional supporting information can be found online in the Supporting Information section

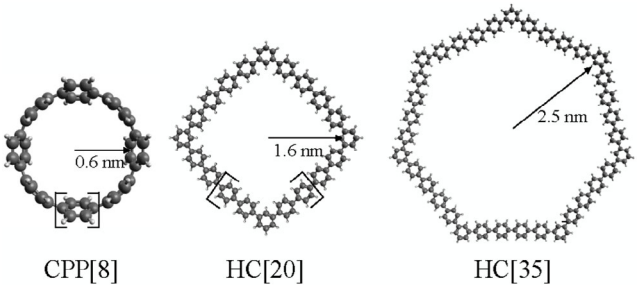

Figure 1. Nanohoops considered in this work. Optimized structures of PFCPP[N] and HC[N] are from Refs. [28] and [29], respectively. The repeated units are enclosed in parenthesis([ ]).

increases with the ring size due to reduction in the radial π conjugation, which is in contrast to linear paraphenylenes, where the gap decreases with increasing length of the chain due to increased linear π conjugation with chain length.[34] Studies suggest that CPPs' charge-transfer electronic coupling is comparable to fullerenes, albeit with lower mobilities owing to higher reorganization energies.[35] PFCPPs, compared to CPPS, have wider HOMO-LUMO gaps, higher reduction potentials, and stronger phosphorescence at low temperatures.[28]

At a single molecular level, CPPs and HCs adsorbed on metal surfaces also exhibit interesting electronic structure at the molecule–metal interface akin to the pioneering work on quantum corraling effects of metal adatoms deposited on metal surfaces.[36] The surface electrons of metals behave as a 2D-electron gas, with a nearly free-electron like parabolic dispersion. These surface electrons, as shown by STM studies, are confined within the nanopores of the surface-deposited nanohoops, leading to the emergence of quantized states. The confinement effects, termed as a molecular quantum corral (MQC) behavior, is similar to the observation for the ring of metal adatoms on metal surfaces.[29,36,37] The molecular scaffold of large nanoporous organic molecules acts as a barrier to the 2D-electron gas leading to the emergence of discrete localized states. The energy levels of these states have been modeled using the particle-in-a-box model, where the box radius is correlated to the molecular-pore dimensions.[29,37][] We, however, note that the theory of quantum corral states is an ongoing area of research due to the increasing exploration of variety of scaffolds—such as metal adatoms, small molecular assemblies, and metal organic frameworks—to create the corral behavior.[1,3,36–41] The nature of the confining potential is a topic of active investigation.[42,43] For purely organic molecules, for which the confining molecular potential has been assumed to be repulsive, the particle-in-a-box model describes the trends in the observed STM resonance voltages very well.[29,37][] This confirms the unbound nature of the MQC states. Despite these interesting observations the usefulness of MQC states toward charge-mobility-based applications is unclear, and their existence in the absence of the metal surface, that is, the molecular origin of such states, remains an open question. It is also unclear if the nanohoops possess any bound nanopore-confined electronic states.

To model the one-particle electronic states of nanohoops corresponding to the attachment of an excess electron, it is necessary to account for many-body polarization effects and exchange interactions in response to the addition of an excess electron. Such computations are challenging due to the large sizes of nanohoops and the need for considering dimers of nanohoops for obtaining electronic charge-transfer couplings. To overcome the computational challenge, we consider a many-body effective potential approach termed as single-pole exchange-correlation (1p-XC), which has been shown to provide accurate electron affinities (EAs) at a computational scaling similar to that of the hybrid density functional methods.[44] The theoretical formulation of 1p-XC is briefly discussed in the computational details section.

Our studies lead to three central results.

1. All organic nanoporous frameworks support the existence of nonvalence anionic states where an excess-electron is bound by long-range polarization forces and the electronic density is confined within the nanopore or away from the molecular scaffold unlike the skeletal-bound states. We term these states as nanopore-bound states, which have a weaker binding energy compared to the skeletal states, and establish that they are a common feature of nanohoops and COFs.

2. The nature of nanopore-bound states is distinct from skeletal-bound states and MQC states. The EAs of the nanopore-bound states first increase and then decrease due to variations in the size of the polarization-induced quantum well. In contrast, with increasing nanohoop size, the EAs of skeletal-bound states systematically reduces while the energy-levels corresponding to the MQC states systematically increases, consistent with repulsive confinement effects.

3. The electron-transfer couplings in nanopore-bound states are consistently larger compared to the skeletal-bound states. As a result, for 1D assemblies of nanohoops, nanopore-bound states exhibit nearly-free-electron (NFE) band-dispersion in several lattice directions, whereas the skeletal-bound states show NFE behavior only in certain lattice directions.

Results and Discussion

To compute the electron affinities, we used the virtual eigenvalues of the single-pole exchange-correlation potential (1p-XC) Hamiltonian

$$\mathbf{H}^{\text{1p-XC}}[\mathbf{D},\omega_0]\,|\phi_p^{\text{1p-XC}}\rangle = \varepsilon_p^{\text{1p-XC}}\,|\phi_p^{\text{1p-XC}}\rangle\,, \tag{1}$$

where $\mathbf{H}^{\text{1p-XC}}$ is the one-particle 1p-XC Hamiltonian given by

$$\mathbf{H}^{\text{1p-XC}} = \mathbf{T} + \mathbf{V}^{\text{ext}} + \mathbf{V}^{\text{H}} + \mathbf{V}^{\text{EXX}} + \mathbf{V}^{\text{1p-C}}[\omega_0]. \tag{2}$$

Here, $\mathbf{T}$ is the kinetic energy operator, $\mathbf{V}^{\text{ext}}$ is the external potential, $\mathbf{V}^{\text{H}}$ is Hartree potential, $\mathbf{V}^{\text{EXX}}$ is the exact-exchange potential, and $\mathbf{V}^{\text{1p-C}}[\omega_0]$ is the single-pole correlation potential, which accounts for many-body polarization effects but has a parametric dependence on ω_0, which is used to model frequency-dependent screened Coulomb interaction via a single-Lorentzian functional form. This parameter-dependent

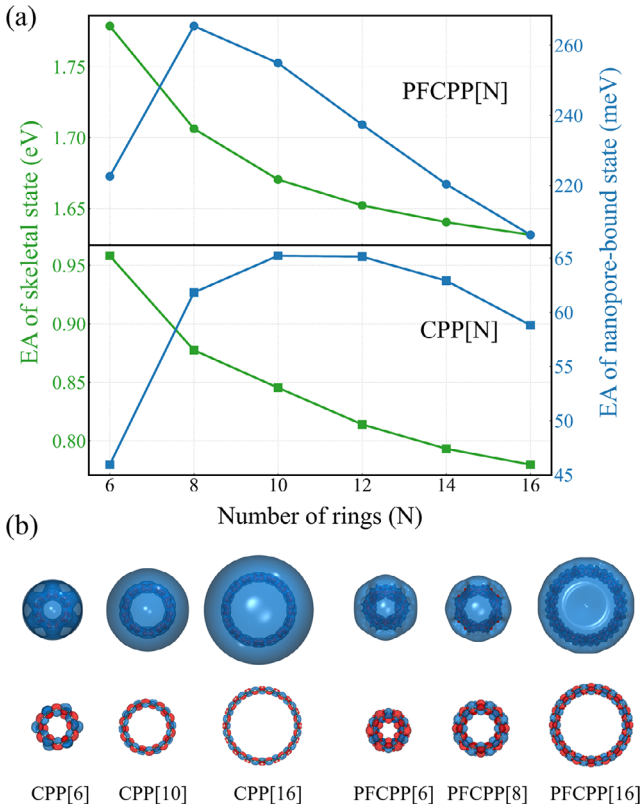

Figure 2. a) EAs of the most stable skeletal and nanopore-bound states obtained using aug-cc-pVDZ+7s7p basis-set. b) Molecular orbital isosurfaces of nanopore-bound (top) and skeletal-bound (bottom) states enclosing 80% electron density.

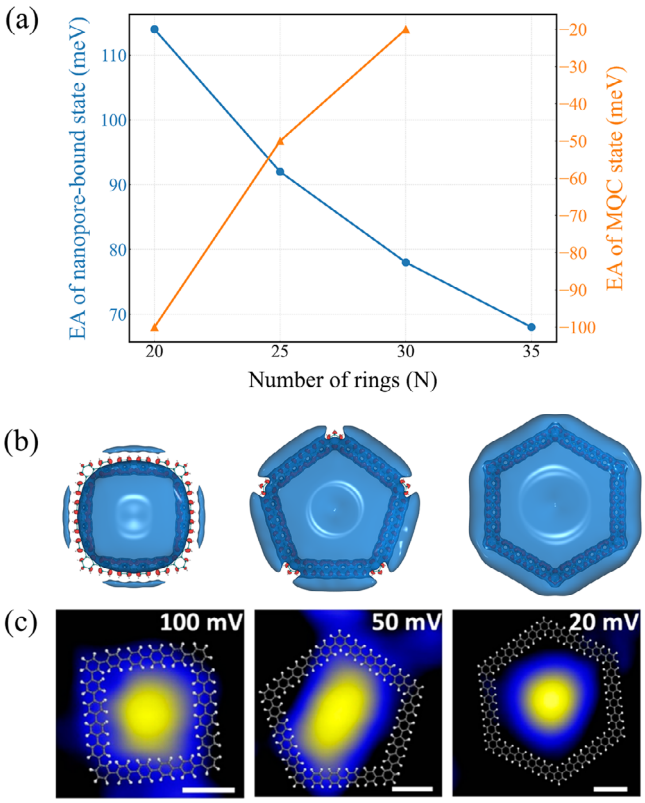

Figure 3. a) EA of the most stable nanopore-bound state of HC[N] obtained using the 1pXC method and the energy-level of the experimentally observed MQC states.[29] For the basis-sets we use cc-pVDZ(+sp) for C, aug-cc-pVDZ(+1s1p) for H and 7s7p7d diffuse function at center of mass. b) Isosurfaces of the nanopore-bound states of HC[N] (N=20, 25, and 30) c) MQC standing wave patterns observed in *dI*/*dV* mode STM images for HC[N](N=20, 25, and 30). The bias voltages (in mV) at which the patterns were observed are indicated in the top right corner. Molecular models are overlaid on the positions of the macrocycle as observed in STM images. Adapted with permission from Ref. [29] (Copyright 2017 American Chemical Society).

dielectric function leads to very efficient computations, but requires a state-specific single-frequency parameter ω_0. This parameter is obtained by fitting against EAs obtained from a higher-level parameter-free approaches such as the random phase approximation (RPA) methods for a particular choice of nanohoop in a series.[45,46] The same ω_0 parameter is then used for all other nanohoops in a given series. The 1p-XC model was shown to provide high accuracy for EAs of solvated-electron systems and fullerene assemblies. For basis-sets, we use the Dunning's augmented correlation-consistent double zeta (aug-cc-pVDZ) basis-sets[47,48] with an extra set of even-tempered 7s7p or 7s7p7d diffuse functions placed at the center of the nanopore(s). These composite basis-sets, denoted as aug-cc-pVDZ + 7s7p/7s7p7d, were previously used to compute EAs of nonvalence anionic states of water clusters, perhalobenzene molecules, and fullerene clusters.[44,46,49] Further details of the optimized ω_0 parameter, its benchmarking, and basis-set studies are provided in the Supporting Information. The maximum error for 1p-XC was 9 meV for monomer's electron affinity, and 7 meV for electronic coupling.

Using the 1p-XC effective potential approach, we computed the variations in EAs for the most stable (i.e., highest EA) nanopore-bound and skeletal-bound states with increasing nanohoop size (i.e., increasing N), see Figures 2 and 3. For nanopore-bound states in CPP the stability of the electron attached state increases (denoted by increasing EA) from 46 meV for CPP[6] to 65 meV for CPP[10], and then decreases from CPP[10]–CPP[16]. A similar trend is observed for PFCPP, where the maximum stability is reached for PFCPP[8] with an EA of 265 meV. For PFCPP[8], in addition to the *s*-type nanopore-bound state shown in Figure 2, we observed an additional degenerate set of *p*-type nanopore-bound states with EA = 13 meV, see Supporting Information. Fluorination increases the EAs of nanopore-bound states by three to four times. For HCs, we observe only a decreasing trend with increasing size as the smallest member in this series, HC[20], already contains 20 phenyl rings.

The existence of a maximum in the EA trend can be traced to the shape of the attractive polarization-potential well in the interior of the nanohoop, see Figure 4. For smaller nanohoops, the well-width is smaller than the larger nanohoops while the well-depth is more compared to the larger nanohoops. With an increase in the nanohoop-size, the well-depth decreases, while the well-width increases. The two competing effects lead to the existence of an optimal-size for attractive confinement of the excess-electron in

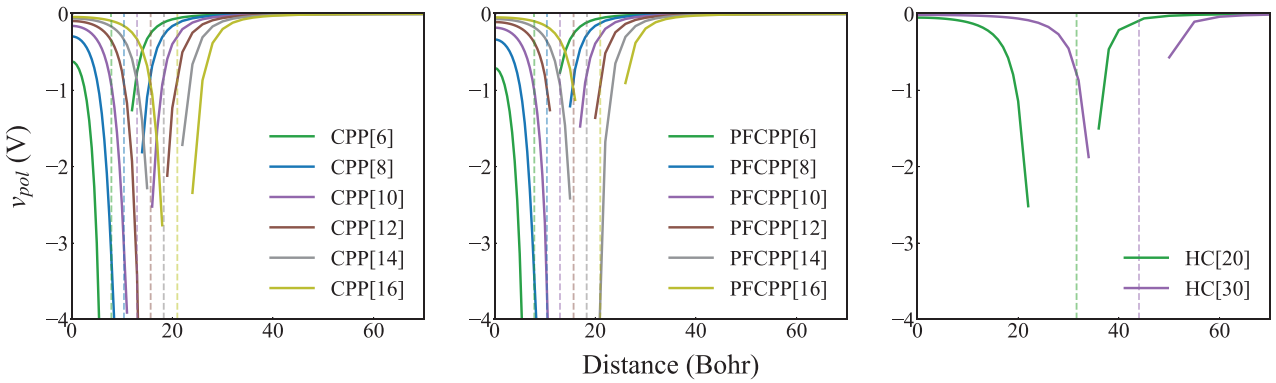

Figure 4. Polarization potential (v_{pol}) along the molecular plane with origin at the center of mass of the molecule. r is the distance from the origin. The potential is computed using the PBE functional.[50] The dashed-lines indicate the nanohoop radius.

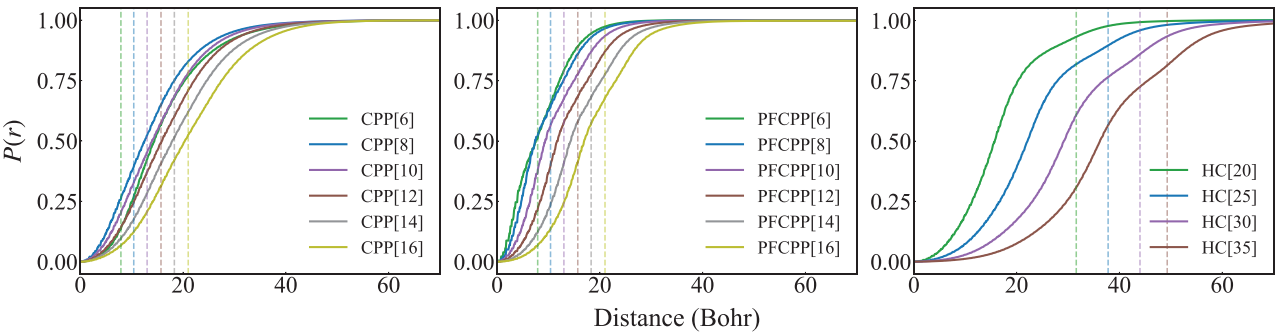

Figure 5. Integrated orbital density, P(r), for a cylinder of radius r with its axis perpendicular to the nanohoop plane and going through the molecular center of mass. Dashed-lines indicate the radius of the nanohoop-skeleton.

the nanopores. This attractive polarization potential in the interior of the nanopores, is central to the emergence of nanopore-bound states. For example, in the absence of the diffuse basis-functions, which span the nanopore region, the nanopore-bound states vanish but the skeletal-bound states are unaffected. The electron binding and the emergence of nanopore-states is therefore polarization induced.

The observed trend in the EAs of nanopore-bound states with nanohoop-size is in contrast to the conventional skeletal-bound electron attachment states and the molecular quantum corral (MQC) states observed at nanohoop/metal interfaces. For example, for the most-stable skeletal-bound state of nanohoops, the EA *always* decreases with increasing size for all the nanohoops, see Figure 2. The stark difference between the nanopore-bound states and skeletal-bound states is evident from their orbital electronic density profiles, the former has a highly diffuse character while the latter is localized on the molecular skeleton. For the MQC states, on the other hand, STM experiments on HC[N] show that the states become more stable (unstable) with increasing (decreasing) size of the nanopore, see Figure 3.[29] This trend is a consequence of MQC states being scattering (or unbound) in nature. The corralling effect is essentially repulsive, leading to MQC states becoming more stable with increasing size of the nanohoop. For an infinite-sized nanohoop, the MQC-state energy-level would approach a vanishing value, whereas the nanopore-bound states would approach a finite positive value of EA. However, we note that for both MQC and nanopore bound states the excess-charge density is nonskeletal in nature, that is, localized in the interior or away from the nanohoop scaffold. It is, however, unclear whether the nanopore-bound states would be modified at the nanohoop/metal interface or whether they are related to the MQC states observed in HC[n] and CPP[n] systems.[29,37]

The nature of the attractive polarization potential also impacts the observed trends in the density profiles of nanopore-bound states, see Figures 2, 3, and 5. The excess-electron density of the nanopore-bound states, consistent with other types of nonvalence states, is located beyond the van der Waals region of the molecular skeleton. For CPP[N] molecules, the majority of the electron density is situated in exterior region of the nanohoop. In contrast, for HC[N], most of the electron density is localized inside the nanopore. For the case of PFCPP[N], the smaller members have most of the density outside the nanopore but the larger members have significant density confined to the nanopore. Additionally, with an increase in the number of rings in PFCPP[N] and HC[N], the electron density shifts away from the center of the nanohoop interior toward the molecular scaffold. This trend is, again, due to the reducing magnitude of the polarization potential at the center of the ring.

To characterize the nature of electron-transport via different electronic-states, we computed the electron-transfer (ET) matrix elements and the corresponding band-dispersion

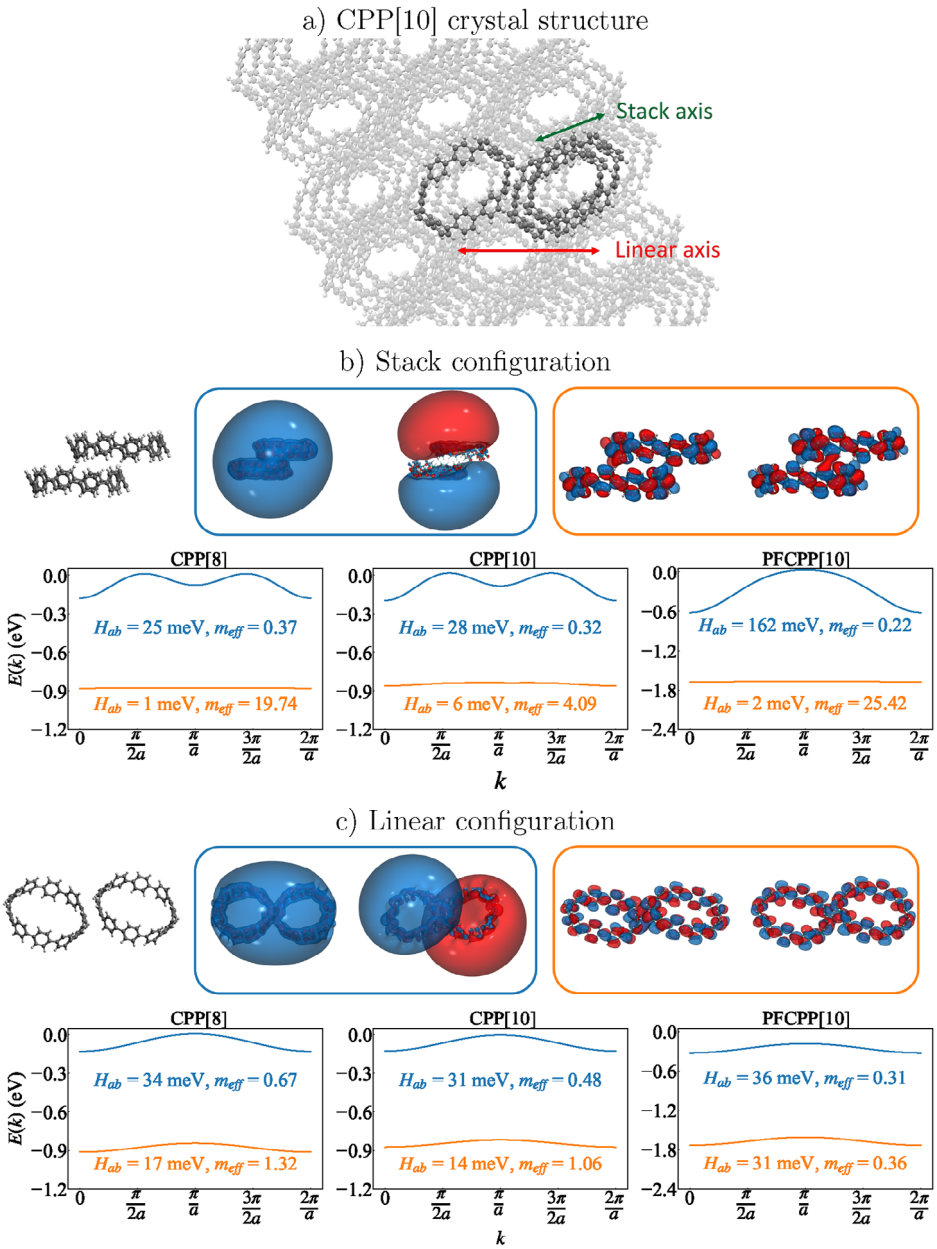

Figure 6. a) CPP[10] crystal structure. b,c) Electronic coupling (H_{ab}) for the dimer, and band dispersion [$E(k)$] and effective mass (m_{eff}) for 1D assemblies in stacked and linear configurations obtained from crystal structures.[28,33,51] The bands correspond to the most-stable skeletal (orange) and nanopore-bound (blue) states. The isosurfaces are the bonding and antibonding hybridized states enclosing 80% electron density.

curves using a tight-binding Hamiltonian for 1D assemblies of the nanohoops, see Figure 6. For the tight-binding model, we considered the first and second-nearest hopping parameters using the ET coupling values. We considered two dimer configurations—stacked and linear—obtained from experimental crystal structures.[28,33,51] For both cases, we find that the nanopore-bound states have consistently higher ET values (25–162 meV) compared to the skeletal-bound states (1–31 meV). For the nanopore-bound states of the stacked configuration, the CPP[8] dimers have coupling values of 28 meV while for PFCPP[8] the ET coupling is about five times higher (162 meV), which indicates a significant impact of fluorination on ET. These ET coupling values are similar to those observed for many high mobility n-type organic acceptor molecules.[52–55] For the linear configurations, the nanopore-bound states of CPP and PFCPP have similar couplings of 31–36 meV, while the skeletal-bound states have smaller couplings of 14–31 meV.

For the bands arising from nanopore-bound states, the effective-mass of the charge-carriers, at the band-minimum, is consistently free-electron like. For the stacking-configuration, the effective masses are in the range of 0.22–0.37 m_e, while for the linear configuration the values are in the range of 0.31–0.67 m_e. For both configurations, the PFCPP[10] has the least effective mass. For the bands arising from the skeletal-bound states we notice a significant anisotropy in the effective

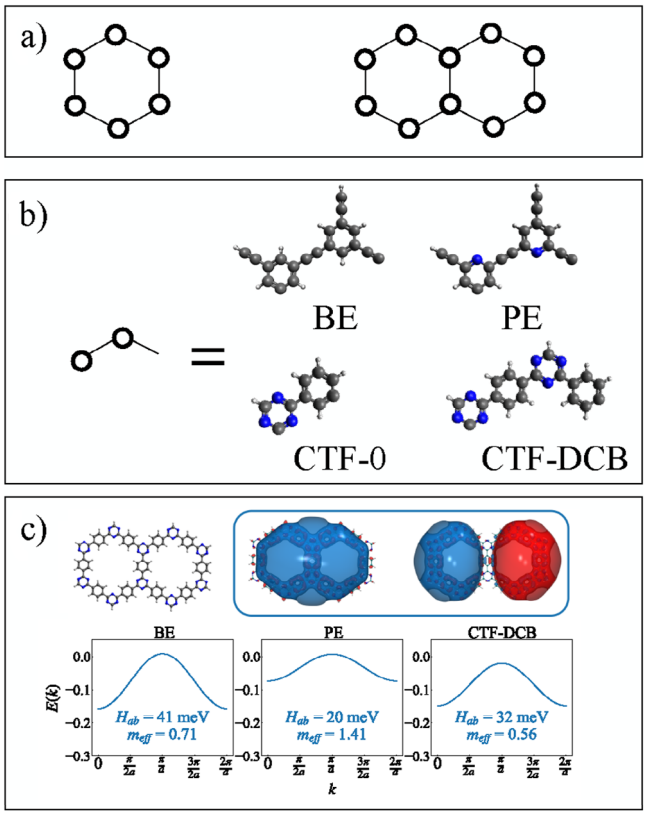

Figure 7. a) Finite (monomer and dimer) units of COFs, b) constituent "lattice-sites" for different COFs. The geometries of the COF units are optimized using the PBE-D3 functional[50,56,57] and def2-TZVPP basis-set.[58] c) Band-dispersion properties for a 1D extended-chain of COF units. The isosurfaces are the bonding and antibonding hybridized states enclosing 80% electron density.

masses. In this case, the stacking-configuration has effective-masses in the range of 4–19 m_e, while the linear-configuration has lower values of 0.4–1.3m_e. Overall, the bands from nanopore-bound state exhibit consistent NFE character and have lower effective masses at the band-minima compared to the skeletal-bound states. However, the nanopore-bound states are higher in energy compared to the bands formed from skeletal-bound states. The band minimum for the nanopore-states is about 1 eV above the maximum of the skeletal-bound state, that is, the conduction-band. The former therefore may not be easily accessible for injecting charge carriers unless broad-excitation wavelength perturbations are used. The nanopore-bound state can enable enhanced transport even if accessed transiently.

At the same time, we note that the energy difference between the most-stable nanopore-bound states and the most-stable skeletal states for CPP nanohoops is about 0.8–0.9 eV, while for PFCPP it is 1.4–1.5 eV. This gap is much smaller than the valence–nonvalence gap of 2.5 eV that was found for C_{60} (the nonvalence states in this case have been referred to as superatomic molecular orbitals).[6,12,53] The larger gap for C_{60} arises from a very stable skeletal-bound state (EA of 2.7 eV). The large EA arises from fused aromatic rings in C_{60}, which are absent in the case of CPP and PFCPP nanohoops. This observation can form an important design principle for engineering molecular frameworks to access the nanopore-bound states.

Our findings for nanohoops appear to be broadly applicable to other nanoporous frameworks such as the 2D COFs. As examples, we consider the finite-sized hexameric analogues of benzene-ethylene (BE) and pyridine-ethylene (PE) COFs and two experimentally synthesized benzene-triazene COFs (CTF-0 and CTF-DCB),[59,60] see Figure 7. For each case, we observed the existence of nanopore-bound states: The EAs of the most-stable nanopore-bound states for monomer units of BE, PE, CTF-0, and CTF-DCB are 74, 33, 5, and 85 meV, respectively. Similar to nanohoops, a size-dependent trend in EA is observed: 5 meV for CTF-0 (which contains 6 rings/unit) to 85 meV for CTF-DCB (containing 12 rings/unit). The ET couplings between units of BE, PE, and CTF-DCB COFs are 41, 20, and 32 meV respectively, as depicted in Figure 7. These studies also suggest that the nanopore-bound states of COFs would have comparable electron transport capabilities as the nanohoops. The stacking of 2D COFs, as observed in the experimentally synthesized material,[16,61] would not affect the existence of the nanopore-bound states. The spatial extent of the nanopore-bound states, however, would extend beyond a single COF layer. We note that some recent studies have shown high electron mobilities of 12.24 $cm^2\ V^{-1}\ s^{-1}$ at temperatures of 2.5 K in COFs although attributed to transport via the skeletal-type states.[62]

Conclusion

In conclusion, the existence of nanopore-bound states in organic nanopores—from nanohoops to COFs—indicates an unexplored common feature of nanopores. The variations in EAs of nanopore-bound states, obtained by using highly efficient many-body methods, affirm their distinct origin from conventional skeletal states and from MQC states observed at nanohoop/metal interfaces. The nearly free-electron character for the effective mass associated with the bands of nanopore-bound states highlights its potential for electronic applications, providing a new channel for electronic confinement and transport.

However, the nanopore-channel, for charge transport, is an excited-state pathway. Its potential for practical realization of electron-transport would require that any (nonadiabatic) couplings with more stable skeletal-bound states be smaller than the electron-transfer couplings. Transient access to the nanopore-bound states may also lead to enhanced electronic transport compared to the transport via more localized skeletal-bound states.

A future research direction would be the experimental observation of the nanopore-bound states. We believe that such states should appear in low-temperature STM experiments and two-photon photoelectron (2PPE) spectroscopy, which have been previously successful in the detection of band-like features in assemblies of other organic molecules.[14,53,63,64] However, it would be important to distinguish these features from MQC-like features that appear usually at low-bias potentials.

Acknowledgements

The authors acknowledge the support of the Department of Atomic Energy (DAE), Government of India, under project no. RTI4003. The authors thank Prof. Pratap Raychaudhuri, Prof. Vaibhav Prabhudesai and Prof. Ravindra Venkatramani for valuable discussions.

Conflict of Interests

The authors declare no conflict of interest.

Data Availability Statement

The data that support the findings of this study are available in the supplementary material of this article.

Keywords: Covalent organic frameworks · Electron transfer · Many-body methods · Nanostructures · Quantum confinement

[1] J. Lobo-Checa, M. Matena, K. Müller, J. H. Dil, F. Meier, L. H. Gade, T. A. Jung, M. Stöhr, *Science* **2009**, *325*, 300.
[2] Y. Pennec, W. Auwärter, A. Schiffrin, A. Weber-Bargioni, A. Riemann, J. Barth, *Nat. Nanotechnol.* **2007**, *2*, 99.
[3] I. Piquero-Zulaica, J. Lobo-Checa, Z. M. A. El-Fattah, J. E. Ortega, F. Klappenberger, W. Auwärter, J. V. Barth, *Rev. Mod. Phys.* **2022**, *94*, 045008.
[4] K. Lee, S. W. Kim, Y. Toda, S. Matsuishi, H. Hosono, *Nature* **2013**, *494*, 336.
[5] V. K. Voora, A. Kairalapova, T. Sommerfeld, K. D. Jordan, *J. Chem. Phys.* **2017**, *147*, 214114.
[6] V. K. Voora, L. S. Cederbaum, K. D. Jordan, *J. Phys. Chem. Lett.* **2013**, *4*, 849.
[7] V. K. Voora, K. D. Jordan, *J. Phys. Chem. Lett.* **2015**, *6*, 3994.
[8] Y.-F. Wang, Z.-R. Li, D. Wu, C.-C. Sun, F.-L. Gu, *J. of Comput. Chem.* **2010**, *31*, 195.
[9] J. P. Rogers, C. S. Anstöter, J. R. Verlet, *Nat. Chem.* **2018**, *10*, 341.
[10] J. N. Bull, J. R. R. Verlet, *Sci. Adv.* **2017**, *3*, 5.
[11] C. Gahl, K. Ishioka, Q. Zhong, A. Hotzel, M. Wolf, *Faraday Discuss.* **2000**, *117*, 191.
[12] M. Feng, J. Zhao, H. Petek, *Science* **2008**, *320*, 359.
[13] M. Feng, J. Zhao, T. Huang, X. Zhu, H. Petek, *Acc. Chem. Res.* **2011**, *44*, 360.
[14] D. B. Dougherty, M. Feng, H. Petek, J. T. Yates, J. Zhao, *Phys. Rev. Lett.* **2012**, *109*, 266802.
[15] R. Jasti, J. Bhattacharjee, J. B. Neaton, C. R. Bertozzi, *J. Am. Chem. Soc.* **2008**, *130*, 17646.
[16] A. P. Côté, A. I. Benin, N. W. Ockwig, M. O'Keeffe, A. J. Matzger, O. M. Yaghi, *Science* **2005**, *310*, 1166.
[17] H. M. El-Kaderi, J. R. Hunt, J. L. Mendoza-Cortés, A. P. Côté, R. E. Taylor, M. O'Keeffe, O. M. Yaghi, *Science* **2007**, *316*, 268.
[18] M. Hermann, D. Wassy, B. Esser, *Angew. Chem., Int. Ed.* **2021**, *60*, 15743.
[19] E. J. Leonhardt, R. Jasti, *Nat. Rev. Chem.* **2019**, *3*, 672.
[20] S. E. Lewis, *Chem. Soc. Rev.* **2015**, *44*, 2221.
[21] K. Sakaushi, M. Antonietti, *Acc. Chem. Res.* **2015**, *48*, 1591.
[22] Y. Yang, K. Börjesson, *Trends Chem.* **2022**, *4*, 60.
[23] O. G. Ziogos, I. Blanco, J. Blumberger, *J. Chem. Phys.* **2020**, *153*, 044702.
[24] H. Guo, Y. Liu, N. Wu, L. Sun, W. Yang, *ChemistrySelect* **2022**, *7*, e202202538.
[25] O. A. Al-Owaedi, *ACS Omega* **2024**, *9*, 10610.
[26] Y. Ni, M. E. Sandoval-Salinas, T. Tanaka, H. Phan, T. S. Herng, T. Y. Gopalakrishna, J. Ding, A. Osuka, D. Casanova, J. Wu, *Chem* **2019**, *5*, 108.
[27] Y.-D. Guo, H.-L. Zeng, L.-Z. Hu, X.-H. Yan, X.-Y. Mou, M.-S. Yang, *Phys. Lett. A* **2018**, *382*, 2763.
[28] H. Shudo, M. Kuwayama, M. Shimasaki, T. Nishihara, Y. Takeda, N. Mitoma, T. Kuwabara, A. Yagi, Y. Segawa, K. Itami, *Nat. Commun.* **2022**, *13*, 3713.
[29] M. Chen, J. Shang, Y. Wang, K. Wu, J. Kuttner, G. Hilt, W. Hieringer, J. M. Gottfried, *ACS Nano* **2017**, *11*, 134.
[30] E. R. Darzi, R. Jasti, *Chem. Soc. Rev.* **2015**, *44*, 6401.
[31] M. R. Golder, R. Jasti, *Acc. Chem. Res.* **2015**, *48*, 557.
[32] M. P. Alvarez, P. M. Burrezo, M. Kertesz, T. Iwamoto, S. Yamago, J. Xia, R. Jasti, J. T. L. Navarrete, M. Taravillo, V. G. Baonza, J. Casado, *Angew. Chem., Int. Ed.* **2014**, *53*, 7033.
[33] J. Xia, J. W. Bacon, R. Jasti, *Chem. Sci.* **2012**, *3*, 3018.
[34] T. Iwamoto, Y. Watanabe, Y. Sakamoto, T. Suzuki, S. Yamago, *J. Am. Chem. Soc.* **2011**, *133*, 8354.
[35] J. B. Lin, E. R. Darzi, R. Jasti, I. Yavuz, K. N. Houk, *J. Am. Chem. Soc.* **2019**, *141*, 952.
[36] M. F. Crommie, C. P. Lutz, D. M. Eigler, *Science* **1993**, *262*, 218.
[37] B. N. Taber, C. F. Gervasi, J. M. Mills, D. A. Kislitsyn, E. R. Darzi, W. G. Crowley, R. Jasti, G. V. Nazin, *J. Phys. Chem. Lett.* **2016**, *7*, 3073.
[38] W. Hu, M. A. Kher-Elden, H. Zhang, P. Cheng, L. Chen, I. Piquero-Zulaica, Z. M. Abd El-Fattah, J. V. Barth, K. Wu, Y.-Q. Zhang, *Nanoscale* **2022**, *14*, 7039.
[39] X. Peng, H. Mahalingam, S. Dong, P. Mutombo, J. Su, M. Telychko, S. Song, P. Lyu, P. W. Ng, J. Wu, et al., *Nat. Commun.* **2021**, *12*, 5895.
[40] F. Klappenberger, D. Kühne, W. Krenner, I. Silanes, A. Arnau, F. J. García de Abajo, S. Klyatskaya, M. Ruben, J. V. Barth, *Nano Lett.* **2009**, *9*, 3509.
[41] G. A. Fiete, E. J. Heller, *Rev. Mod. Phys.* **2003**, *75*, 933.
[42] A. I. Rahachou, I. V. Zozoulenko, *Phys. Rev. B* **2004**, *70*, 233409.
[43] A. M. Othman, M. A. Kher-Elden, I. Piquero-Zulaica, J. V. Barth, M. A. Hassan, M. Farouk, Z. M. Abd El-Fattah, *Phys. Rev. B* **2023**, *108*, 205409.
[44] R. Tyagi, V. K. Voora, *J. Phys. Chem. Lett.* **2024**, *15*, 1218.
[45] V. K. Voora, S. G. Balasubramani, F. Furche, *Phys. Rev. A* **2019**, *99*, 012518.
[46] V. K. Voora, *J. Phys. Chem. Lett.* **2020**, *12*, 433.
[47] J. Dunning, H. Thom, *J. Chem. Phys.* **1989**, *90*, 1007.
[48] R. A. Kendall, J. Dunning, Thom H., R. J. Harrison, *J. Chem. Phys.* **1992**, *96*, 6796.
[49] V. P. Vysotskiy, L. S. Cederbaum, T. Sommerfeld, V. K. Voora, K. D. Jordan, *J. Chem. Theory Comput.* **2012**, *8*, 893.
[50] J. P. Perdew, K. Burke, M. Ernzerhof, *Phys. Rev. Lett.* **1996**, *77*, 3865.
[51] J. M. Van Raden, E. J. Leonhardt, L. N. Zakharov, A. Pérez-Guardiola, A. J. Pérez-Jiménez, C. R. Marshall, C. K. Brozek, J. C. Sancho-García, R. Jasti, *J. Org. Chem.* **2020**, *85*, 129.
[52] T. Okamoto, S. Kumagai, E. Fukuzaki, H. Ishii, G. Watanabe, N. Niitsu, T. Annaka, M. Yamagishi, Y. Tani, H. Sugiura, T. Watanabe, S. Watanabe, J. Takeya, *Sci. Adv.* **2020**, *6*, eaaz0632.
[53] J. Zhao, M. Feng, J. Yang, H. Petek, *ACS Nano* **2009**, *3*, 853.
[54] S. Kumagai, H. Ishii, G. Watanabe, C. P. Yu, S. Watanabe, J. Takeya, T. Okamoto, *Acc. Chem. Res.* **2022**, *55*, 660.
[55] V. Coropceanu, Y. Li, Y. Yi, L. Zhu, J.-L. Brédas, *MRS bulletin* **2013**, *38*, 57.
[56] S. Grimme, J. Antony, S. Ehrlich, H. Krieg, *J. Chem. Phys.* **2010**, *132*, 154104.

[57] S. Grimme, S. Ehrlich, L. Goerigk, *J. Comput. Chem.* **2011**, *32*, 1456.
[58] F. Weigend, R. Ahlrichs, *Phys. Chem. Chem. Phys.* **2005**, *7*, 3297.
[59] D. Kong, X. Han, J. Xie, Q. Ruan, C. D. Windle, S. Gadipelli, K. Shen, Z. Bai, Z. Guo, J. Tang, *ACS Catal.* **2019**, *9*, 7697.
[60] T. Sun, Y. Liang, Y. Xu, *Angew. Chem., Int. Ed.* **2022**, *61*, e202113926.
[61] N. Keller, T. Bein, *Chem. Soc. Rev.* **2021**, *50*, 1813.
[62] S. Wang, L. Da, J. Hao, J. Li, M. Wang, Y. Huang, Z. Li, Z. Liu, D. Cao, *Angew. Chem. Int. Ed.* **2021**, *60*, 9321.
[63] X.-Y. Zhu, G. Dutton, D. P. Quinn, C. D. Lindstrom, N. E. Schultz, D. G. Truhlar, *Phys. Rev. B* **2006**, *74*, 241401.
[64] T. Vondrak, X.-Y. Zhu, *J. Phys. Chem. B* **1999**, *103*, 3449.

Manuscript received: November 25, 2024
Revised manuscript received: February 25, 2025
Accepted manuscript online: March 10, 2025
Version of record online: March 23, 2025